

Specific heat of $\text{Ca}_{0.32}\text{Na}_{0.68}\text{Fe}_2\text{As}_2$ single crystals: Unconventional s_{\pm} multiband superconductivity with intermediate repulsive interband coupling and sizable attractive intraband couplings

S. Johnston,^{1,2,3} M. Abdel-Hafiez,¹ L. Harnagea,¹ V. Grinenko,¹ D. Bombor,¹ Y. Krupskaya,¹ C. Hess,¹ S. Wurmehl,¹ A. U. B. Wolter,¹ B. Büchner,^{1,4} H. Rosner,^{5,1} and S.-L. Drechsler¹

¹Leibniz-Institute for Solid State and Materials Research, (IFW)-Dresden, D-01171 Dresden, Germany

²Department of Physics and Astronomy, University of British Columbia, Vancouver, British Columbia, Canada V6T 1Z1

³Quantum Matter Institute, University of British Columbia, Vancouver, British Columbia, Canada V6T 1Z4

⁴Physical Department, University of Technology Dresden, Germany

⁵Max-Planck Institute for Chemical Physics of Solids (MPI-CPfS), Dresden, Germany

(Received 13 November 2013; revised manuscript received 14 February 2014; published 14 April 2014)

We report a low-temperature specific heat study of high-quality single crystals of the heavily hole-doped superconductor $\text{Ca}_{0.32}\text{Na}_{0.68}\text{Fe}_2\text{As}_2$. This compound exhibits bulk superconductivity with a transition temperature $T_c \approx 34$ K, which is evident from the magnetization, transport, and specific heat measurements. The zero-field data manifest a significant electronic specific heat in the normal state with a Sommerfeld coefficient $\gamma \approx 53$ mJ/mol K². Using a multiband Eliashberg analysis, we demonstrate that the dependence of the zero-field specific heat in the superconducting state is well described by a three-band model with an unconventional s_{\pm} pairing symmetry and gap magnitudes Δ_i of approximately 2.35, 7.48, and -7.50 meV. Our analysis indicates a non-negligible attractive intraband coupling, which contributes significantly to the relatively high value of T_c . The Fermi surface averaged repulsive and attractive coupling strengths are of comparable size and outside the strong coupling limit frequently adopted for describing high- T_c iron pnictide superconductors. We further infer a total mass renormalization of the order of five, including the effects of correlations and electron-boson interactions.

DOI: [10.1103/PhysRevB.89.134507](https://doi.org/10.1103/PhysRevB.89.134507)

PACS number(s): 74.25.Bt, 74.25.Dw, 74.25.Jb, 65.40.Ba

I. INTRODUCTION

Among the still increasing number of iron pnictide and chalcogenide based superconductors, the hole doped systems within the $A_{1-x}B_x\text{Fe}_2\text{As}_2$ (A -122) family, where $A = \text{Ba}, \text{Sr}, \text{Ca}$ and $B = \text{K}, \text{Na}$, and other alkaline elements, have attracted considerable attention. This is due to the availability of large stable high-quality single crystals necessary for an accurate determination of many physical properties. However, within this family, the pure Ca-122 and its derived Na-doped systems stand out in a number of ways when compared to their pure and K or Na-doped Ba-122 and Sr-122 counterparts.

The first striking difference is the variation of T_c with respect to doping. For example, the “optimal” doping concentrations, where the highest values of T_c are achieved, are rather different. In Ba-122, optimal doping occurs at $x \approx 0.3$ to 0.4 for K doping ($T_c \approx 38.5$ K) [1] and $x \approx 0.4$ for Na doping ($T_c \approx 34$ K) [2]. These concentrations are significantly smaller than the optimal $x \approx 0.75$ ($T_c \approx 35$ K) for Na-doped Ca-122 [3]. The T_c values for comparable nominal doping concentrations also differ significantly. At $x \approx 0.5$ K-doped, Ba-122 exhibits $T_c \approx 36$ K versus a $T_c \approx 18$ to 19 K for Na-doped Ca-122 [4,5], while for the strongly doped case near $x \approx 0.7$ this ratio is reversed. In general, the asymmetry of the electron (Co) and hole (Na) doped phase diagram, known also for other A -122 superconductors, is most pronounced for the Ca-122 family [6]. La and P co-doping of Ca-122 also yields the highest value of T_c (≈ 45 K) among the A -122 derived superconductors [7].

Another difference concerns the weakly anisotropic upper critical field. Resistivity data for optimally [3] and undoped (under pressure) [8] single crystals of Na-doped Ca-122 (anisotropy ratios of 1.85 ± 0.05 and 1.2, respectively) suggest

that this system possesses the smallest out-of-plane anisotropy observed so far among the iron pnictides.

The phonon spectrum in Ca-122 also displays some peculiarities. Anomalously large phonon linewidths have been observed by inelastic neutron scattering, which have been interpreted in terms of an enhanced electron-phonon (e-ph) interaction [9] relative to other pnictides. This raises the question of a possible role for the e-ph interaction in establishing or promoting superconductivity in this subgroup [10]. These observations, combined with the presence of a pseudogaplike phase in under- and optimally electron doped single crystals [11], and other unusual features such as a topological Fermi surface (Lifshitz) transition [12], make the Ca-122 systems a rather special subgroup of pnictides deserving a systematical investigation.

From both theoretical (electronic structure and Eliashberg-theory based analysis) and experimental sides (ARPES) there is clear evidence that most iron pnictide superconductors cannot be described quantitatively within the popular two-band model and generalizations to three- or four-band models are necessary [1,13–15]. Another issue under debate is the total coupling strength, be it in the weak or intermediate versus strong coupling regimes, and the related size of the mass renormalization in the normal state. In the present paper, we will show that $\text{Ca}_{0.32}\text{Na}_{0.68}\text{Fe}_2\text{As}_2$ with respect to these issues is also distinct from the nearly optimal doped Ba- and Sr-122 systems.

In this context, specific heat measurements are a useful probe to provide key information such as the upper critical field, the magnitude of the specific heat jump $\Delta C_p/T_c$, and the linear in temperature (T) specific heat (Sommerfeld) coefficient in the normal state γ_{el} . The latter reflects the strength of the electron-boson coupling possibly responsible

for the superconductivity. Furthermore, the low-temperature (low- T) specific heat can evaluate the presence or absence of nodes in the superconducting order parameter. In this paper, we present low- T specific heat measurements on single crystals of hole-doped $\text{Ca}_{0.32}\text{Na}_{0.68}\text{Fe}_2\text{As}_2$. By performing a detailed multiband Eliashberg analysis of the data we derive three distinct gap values for this system and conclude a total Fermi surface averaged coupling strength in the intermediate coupling regime. We further find evidence for a sizable intraband component to pairing, which is manifest as a pronounced knee in the zero field data as a function of temperature. Although, such investigations have been performed for analogous compounds (i.e., K and Na-doped BaFe_2As_2) [1,16,17], these studies are lacking for the Na-doped CaFe_2As_2 systems. Such systematics are needed in order to further clarify the differences between these structurally similar systems, and to determine to what extent the magnitude and symmetries of the superconducting order parameter, as well as the magnitude of the specific heat jump (coupling strength) at T_c , are sensitive to the different chemical compositions of the A -122 families.

II. METHODS

A. Experimental

In the present work, we study thermodynamic properties of single crystals of the parent compound CaFe_2As_2 and heavily hole-doped $\text{Ca}_{0.32}\text{Na}_{0.68}\text{Fe}_2\text{As}_2$. Single crystals of the parent system were obtained using a high-temperature solution-growth technique with Sn as a flux, similar to the one described in Ref. [6]. Single crystals of $\text{Ca}_{0.32}\text{Na}_{0.68}\text{Fe}_2\text{As}_2$ were grown using NaAs as a flux. The starting composition was selected as $\text{Ca}_{0.5}\text{Na}_{0.5}\text{Fe}_2\text{As}_2$: NaAs = 1 : 2 in a molar ratio. The mixture of the precursors CaAs, Fe_2As and NaAs were loaded in an alumina crucible. The crucible was sealed under argon atmosphere in a Nb container enclosed in an evacuated quartz ampoule. The precursor mixture was slowly heated to 1373 K, held there for 24 hours to ensure homogenization, and then gradually cooled down to 873 K at a rate of 3 K/h, followed by rapid cooling to room temperature.

The phase purity of the resulting single crystals was investigated with x-ray diffraction. The chemical composition was accessed by using a scanning electron microscope (SEM-Philips XL 30) equipped with an energy dispersive x-ray (EDX) spectroscopy probe. Generally, the samples proved to be single phase. To determine the chemical composition of Na-doped samples, we performed an EDX analysis for different samples from the same batch and at different locations on each particular sample. Similar to the previously reported data [3], the samples proved to be relatively homogeneous with a standard deviation in the Na concentration ranging between 0.03 and 0.06. The magnetization measurements were performed using a superconducting quantum interference device magnetometer (MPMS-XL5) from Quantum Design. The temperature dependence of the electric resistivity of the samples was measured using a standard four-contact technique. The contacts were attached with silver epoxy such that the electrical current flowed parallel to the ab plane. The heat capacity was measured with a Physical Property Measurement System (PPMS) from Quantum Design using

a thermal relaxation technique down to 1.8 K and magnetic fields up to 9 T applied along the crystallographic c axis.

B. Theory

1. Electronic structure calculations

Scalar-relativistic density functional (DFT) electronic structure calculations were performed using the full-potential FPLO code [18], version FPLO9.01-35. The parametrization of Perdew-Wang [19] was chosen for the exchange-correlation potential within the local density (LDA). The calculations were carried out on a well converged mesh of 8632 k points in the irreducible wedge of the Brillouin zone ($50 \times 50 \times 50$ mesh) to ensure a high resolution for details in the electronic density of states. The partial Ca substitution with Na was modeled within the virtual crystal approximation (VCA) [20].

2. Multiband Eliashberg analysis

We calculate the change in the electronic specific heat $\Delta C_{\text{el}}(T)$ using multiband Eliashberg theory. It is given by $\Delta C_{\text{el}}(T) = T \partial^2(\Delta F)/\partial T^2$, where $\Delta F = F_N - F_S$ is the difference between the free energy of the system in the normal and superconducting states. The change in free energy can be expressed in terms of the mass renormalization $Z_i(\omega_n)$ and anomalous self-energy $\phi_i(\omega_n)$ on the Matsubara frequency axis [21]:

$$\Delta F = -\frac{\pi}{\beta} \sum_{i,n} N_i(0) \left(|\omega_n| [Z_i^N(\omega_n) - 1] - 2 \frac{\omega_n^2 \{ [Z_i^S(\omega_n)]^2 - 1 \} + \phi_i^2(\omega_n)}{|\omega_n| + \sqrt{\omega_n^2 [Z_i^S(\omega_n)]^2 + \phi_i^2(\omega_n)}} + \frac{\omega_n^2 Z_i^S(\omega_n) [Z_i^S(\omega_n) - 1] + \phi_i^2(\omega_n)}{\sqrt{\omega_n^2 [Z_i^S(\omega_n)]^2 + \phi_i^2(\omega_n)}} \right).$$

Here, $\beta = 1/k_b T$ is the inverse temperature, $N_i(0)$ is the single-particle partial density of states (DOS) of band i at the Fermi level, and the superscripts N and S denote the normal and superconducting states, respectively. The mass renormalization and anomalous self-energy are obtained by solving the multiband Eliashberg equations. They are [13]

$$Z_i(\omega_n) \Delta_i(\omega_n) = \frac{\pi}{\beta} \sum_{m,j} D_{ij}(\omega_n - \omega_m) \frac{\Delta_j(\omega_m)}{\sqrt{\omega_n^2 + \Delta_j^2(\omega_m)}} \quad (1)$$

and

$$Z_i(\omega_n) = 1 + \frac{\pi}{\beta} \sum_{m,j} D_{ij}(\omega_n - \omega_m) \frac{(\omega_m/\omega_n) Z_j(\omega_m)}{\sqrt{\omega_n^2 + \Delta_j^2(\omega_m)}}, \quad (2)$$

where ω_n and ω_m are fermion Matsubara frequencies, $\Delta_i(\omega_n) = \phi_i(\omega_n)/Z_i(\omega_n)$ is the gap function, and

$$D_{ij}(\omega_n - \omega_m) = \lambda_{ij} \int_0^\infty dv \frac{2v B_{ij}(v)}{(\omega_n - \omega_m)^2 + v^2}. \quad (3)$$

The dimensionless coupling strength λ_{ij} parameterizes the coupling strength to the bosonic spectrum $B_{ij}(v)$, which has both intra- [$B_{ii}(v)$] and interband [$B_{ij}(v)$] components. Our

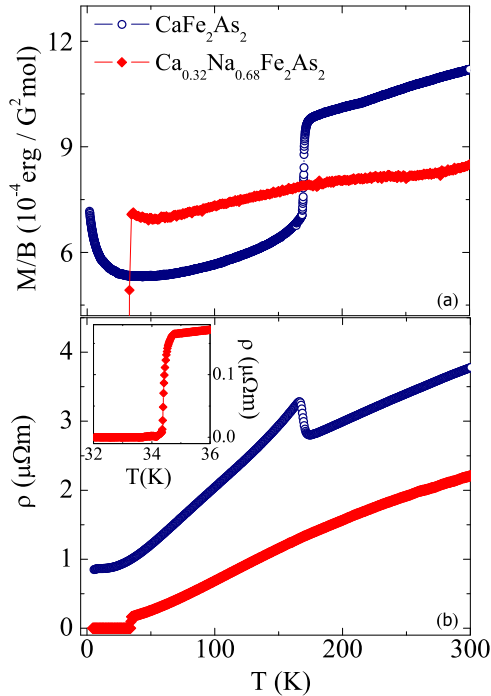


FIG. 1. (Color online) (a) The T dependence of the magnetization of CaFe_2As_2 and $\text{Ca}_{0.32}\text{Na}_{0.68}\text{Fe}_2\text{As}_2$ single crystals, measured under an applied magnetic field of 1 T parallel to the crystallographic basal plane in zero-field cooled conditions. (b) T dependence of the in-plane electrical resistivity in zero field up to 300 K. The inset presents a zoom of the resistivity data around T_c for the $\text{Ca}_{0.32}\text{Na}_{0.68}\text{Fe}_2\text{As}_2$ sample.

specific choice for the spectral densities and coupling constants are given in the following section. Finally, in order to obtain the value of the superconducting gap measured by spectroscopies, the self-energies are analytically continued to the real axis using the method of Ref. [22].

III. RESULTS

A. Magnetization and resistivity

Figure 1 shows the T dependence of the magnetization and resistivity of the parent compound CaFe_2As_2 and of $\text{Ca}_{0.32}\text{Na}_{0.68}\text{Fe}_2\text{As}_2$ single crystals. Figure 1(a) presents the T dependence of the magnetization measured in zero field-cooled conditions and in a magnetic field of 1 T applied parallel to the ab plane. The parent compound shows a combined spin-density-wave (SDW) and structural transition near 169 K, in good agreement with previous reports [6,23]. The first-order SDW/structural transition is completely suppressed upon 68% substitution of Ca by Na and superconductivity appears at $T_c \approx 34$ K. Figure 1(b) shows the in-plane resistivity data for the samples. The parent compound exhibits metallic behavior over the entire temperature range with a prominent anomaly at 169 K, in agreement with the magnetization data. In the Na-doped sample, the SDW/structural anomaly is completely suppressed below $x \approx 0.5$. However, near $x \approx 0.7$, optimal doping is reached where T_c is largest. A sharp superconducting transition is clearly seen at $T_c^{\text{on}} \approx 34.6$ K (90% of the normal state resistivity) with $\Delta T_c = 0.2$ K. The residual resistivity

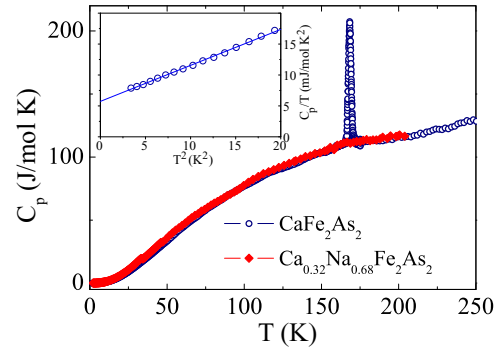


FIG. 2. (Color online) The temperature dependence of the specific heat C_p measured in zero-field conditions for CaFe_2As_2 and $\text{Ca}_{0.32}\text{Na}_{0.68}\text{Fe}_2\text{As}_2$. The inset shows the low-temperature behavior of C_p/T as a function of T^2 . The straight lines are the linear fits to $C_p/T = \gamma + \beta T^2$ (see text).

is $\rho(36 \text{ K}) \approx 17 \mu\Omega\cdot\text{cm}$ and the residual resistivity ratio (RRR) is found to be $\rho(300 \text{ K})/\rho(36 \text{ K}) = 12.8$. These values are similar to those reported for the other hole-doped A -122 systems [24–26], indicating a reasonably good quality of our single crystals.

B. Specific heat

The temperature dependence of the zero-field specific heat for the parent compound and the Na-doped sample are shown in Fig. 2. Here, again, a sharp SDW/structural transition is observed only for the parent compound. The anomaly associated with the structural and magnetic transition is absent in the Na doped sample. Instead, a jump in the specific heat associated with the superconducting phase transition is observed at 34 K (see Fig. 3).

At low T , the data of the parent compound can be fitted to $C_p/T = \gamma + \beta T^2$, where γ and β are the electronic and phononic coefficients of the specific heat, respectively (see inset to Fig. 2). The γ_{el} value for the parent compound is found

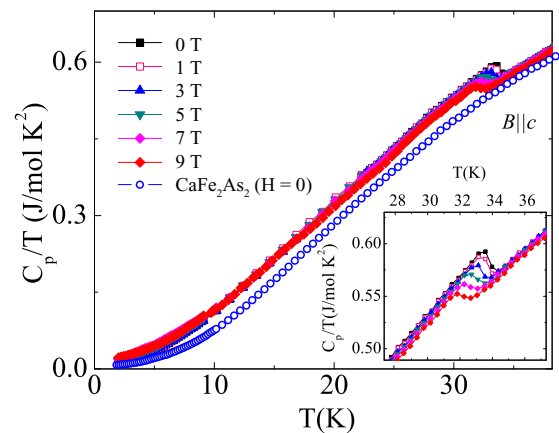


FIG. 3. (Color online) The T dependence of the specific heat C_p/T of $\text{Ca}_{0.32}\text{Na}_{0.68}\text{Fe}_2\text{As}_2$ single crystal measured in magnetic fields applied along the crystallographic c axis. For reference, the specific heat of CaFe_2As_2 measured in zero-field conditions is also shown. The inset shows C_p/T of $\text{Ca}_{0.32}\text{Na}_{0.68}\text{Fe}_2\text{As}_2$ near T_c .

to be around 5.4 mJ/mol K^2 , which is in agreement with the values ranging between 4.7 and 8.2 mJ/mol K^2 reported previously [27,28]. The phononic coefficient β is found to be 0.508 mJ/mol K^4 . Using the relation $\theta_D = (12\pi^4 RN/5\beta)^{1/3}$, where R is the molar gas constant and $N = 5$ is the number of atoms per formula unit, we obtain a Debye temperature $\theta_D = 267 \text{ K}$, which agrees reasonably well with previously reported data [28].

Figure 3 summarizes the T -dependent specific heat measured in various magnetic fields for the $\text{Ca}_{0.32}\text{Na}_{0.68}\text{Fe}_2\text{As}_2$ sample, together with the zero-field measurements of the parent compound. The inset shows the specific heat data in the vicinity of the superconducting transition, where a pronounced jump is observed at T_c . In order to determine T_c for each field, an entropy conserving construction has been used [29].

For further analysis, knowledge of the electronic contribution to the specific heat C_{el} of the $\text{Ca}_{0.32}\text{Na}_{0.68}\text{Fe}_2\text{As}_2$ is required. Since this compound is nonmagnetic, the total specific heat C_{tot} is a sum of the electronic C_{el} and the lattice contributions C_{ph} . In the case of many superconductors, C_{ph} is typically estimated by suppressing the superconducting transition in high magnetic fields. However, this option is not available here due to the high value of the upper critical field. As an alternative, we have estimated C_{ph} for the doped sample from the data for the nonsuperconducting parent compound CaFe_2As_2 using a procedure similar to Ref. [1].

The parent compound exhibits a long-range magnetic order of the AFM-type paired with SDW formation around 169 K , which suggests a likely magnetic contribution to its specific heat. However, a recent inelastic neutron scattering study has revealed that the low-energy spin-wave excitations in the magnetically ordered state are gapped by $\sim 6.9 \text{ meV}$ ($\sim 80 \text{ K}$) in CaFe_2As_2 [30]. Therefore magnetic contributions to the specific heat should be negligible for $T < 40 \text{ K}$ to a first approximation. It is therefore reasonable to assume that the total specific heat consists of only C_{el} and C_{ph} in this temperature range. Furthermore, we expect the phonon contribution to specific heat to be similar in the parent and Na-doped systems. This can be justified empirically. The phonon density of states in CaFe_2As_2 and the related system $\text{Ca}_{0.6}\text{Na}_{0.4}\text{Fe}_2\text{As}_2$ have been measured and it was found that below 12 meV the phonon DOS is unchanged in the two samples [9]. This indicates that the energies of the low-energy acoustic modes that determine C_{ph} are not significantly affected by Na doping. This is further supported by the fact that the lattice parameters in the doped and parent compounds are similar [9]. Furthermore, for $T > T_c$, our specific heat data for the $\text{Ca}_{0.32}\text{Na}_{0.68}\text{Fe}_2\text{As}_2$ and CaFe_2As_2 samples are comparable, confirming similar phonon contributions to the specific heat of both samples. The CaFe_2As_2 data therefore allow us to estimate C_{ph} , which can then be subtracted from the specific heat of our Na-doped sample. A similar approach has been successfully applied in the cases of electron- and hole-doped BaFe_2As_2 [16,31].

In order to determine the phononic contribution, we assume

$$C_{ph}^{\text{CaFe}_2\text{As}_2} = C_{tot}^{\text{CaFe}_2\text{As}_2} - C_{el}^{\text{CaFe}_2\text{As}_2},$$

where $C_{el}^{\text{CaFe}_2\text{As}_2} = \gamma_{el}T$. We further assume that the temperature dependence of the phononic contribution to the heat

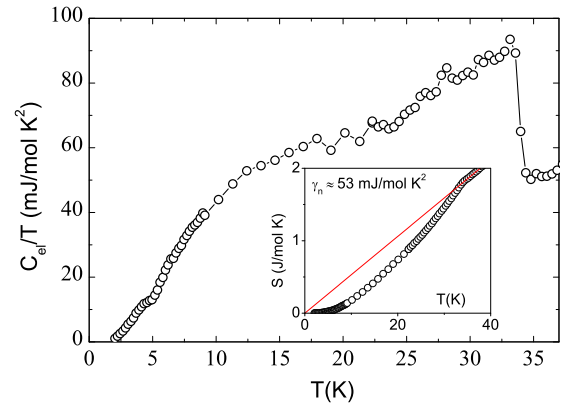


FIG. 4. (Color online) The electronic specific heat of $\text{Ca}_{0.32}\text{Na}_{0.68}\text{Fe}_2\text{As}_2$ after subtracting the phonon contribution as a function of reduced temperature $t = T/T_c$. In the inset, the normal and superconducting state entropies are shown.

capacities of $\text{Ca}_{0.32}\text{Na}_{0.68}\text{Fe}_2\text{As}_2$ and CaFe_2As_2 are the same, as discussed above. Then the electronic specific heat of the superconducting (SC) sample can be represented by

$$C_{el}^{\text{SC}}/T = C_{tot}^{\text{SC}}/T - fC_{ph}^{\text{CaFe}_2\text{As}_2}/T. \quad (4)$$

The scaling factor f has been introduced to account for the difference in the atomic compositions of the parent and hole-doped compounds as well as possible experimental errors in the absolute value of the specific heat, which are of several percent. The value of f was determined from the requirement that the normal and superconducting state entropies at T_c be equal, i.e., $\int_0^{T_c} (C_{el}/T) dT = \gamma_n T_c$, where γ_n is the normal state electronic specific heat coefficient for the doped superconducting sample. We found that the entropy conservation criterion is satisfied for $f = 0.95$ (see inset in Fig. 4).

The resulting C_{el}/T for $\text{Ca}_{0.32}\text{Na}_{0.68}\text{Fe}_2\text{As}_2$ is presented in the main panel of Fig. 4. The procedure yields $T_c = 33.9 \text{ K}$ and a jump in C_{el}/T at T_c of $\approx 39 \text{ mJ/mol K}^2$. Generally, this value is higher than in the case of the electron-doped Ba-122 compounds [32] and respectively smaller compared to the hole-doped Ba-122 compounds [16,33]. The value of the specific heat jump at T_c obtained for this material scales relatively well with its T_c in light of the recent results for the pnictide superconductors [17,34,35].

The obtained high value of $\gamma_n = 53 \text{ mJ/mol K}^2$ for $\text{Ca}_{0.32}\text{Na}_{0.68}\text{Fe}_2\text{As}_2$ as shown in Fig. 4 is comparable to that for other members of the hole-doped A-122 series. From $\gamma_n = 53 \text{ mJ/mol K}^2$, we estimate $\Delta C_{el}/\gamma_n T_c = 0.96$, which is smaller than the prediction of the weak coupling BCS theory ($\Delta C_{el}/\gamma_n T_c = 1.43$) [36]. Taking into account the fact that the superconducting transition is relatively sharp in $\text{Ca}_{0.32}\text{Na}_{0.68}\text{Fe}_2\text{As}_2$, a distribution in T_c or the presence of impurity phases cannot explain the reduced value of the universal parameter (relevant in the single-band weak-coupling case, only). In our case, however, this reduction is explained by the presence of multiple SC gaps, which can reduce the dimensionless jump parameter in $\text{Ca}_{0.32}\text{Na}_{0.68}\text{Fe}_2\text{As}_2$, as evidenced in other A-122 systems [16,31,37,38]. Further evidence for a multigap scenario in this compound is given by

the significant hump around 13 K in our C_{el}/T versus T data (see Fig. 4), which we will discuss in greater detail below.

C. Multiband Eliashberg analysis

We now undertake an analysis of the specific heat in the superconducting state using multiband Eliashberg theory and calculate the change in electronic specific heat as outlined in Sec. II B 2. To model the self-energies, we assume an effective three-band model. One can associate two of the bands ($i = 1, 2$) with different hole pockets and one band ($i = 3$) with both electron pockets, which provide a single band by reasons of symmetry. (However, other assignments are possible, which we discuss in greater detail below.) We further assume that the intraband scattering is dominated by the attractive ($\lambda_{ii} > 0$) e-ph interaction while the interband scattering is dominated by a repulsive ($\lambda_{ij} < 0$) spin fluctuation mediated interaction [1]. [Note that the negative sign for λ_{ij} only enters into Eq. (1) while in Eq. (2) all λ_{ij} enter with a +ve sign.] The bosonic spectral densities $B_{ii}(\nu) = B_{ph}(\nu)$ and $B_{ij}(\nu) = B_{sf}(\nu)$, respectively, are shown in Fig. 5(a). The phonon spectrum is taken from Ref. [9], while the spin fluctuation spectrum is assumed to have the form $B_{sf}(\nu) = \Omega_{sf}\nu/(\nu^2 + \Omega_{sf}^2)$ ($\Omega_{sf} = 20$ meV) [13,39]. In both cases, $B_{ij}(\nu)$ has been normalized such that $\int_0^{\omega_c} d\nu 2B_{ij}(\nu)/\nu = 1$ and the spin fluctuation spectrum has been cut off for $\nu > \omega_c = 100$ meV. We solve Eqs. (1) and (2) self-consistently assuming an s_{\pm} gap symmetry and treating the values of λ_{ij} and $N_i(0)$ as adjustable parameters.

The T dependence of the gaps Δ_i at the $n = 1$ Matsubara frequency are shown in Fig. 5(b). Our model gives

$T_c^{\text{fit}} = 33.6$ K and the low temperature ($T = 0.5$ K) gaps are $\Delta_i(\omega_n = \pi/\beta) = 7.16, 2.36,$ and -7.20 meV. The corresponding spectroscopic gaps on the real axis are $\Delta_i = 7.48, 2.35,$ and -7.5 meV, respectively. The non-BCS temperature dependence for the smallest gap Δ_2 is a typical feature of the outer FSS (h_3) which are very weakly coupled to the remaining “strongly” coupled FSSs h_1, h_2 and e_1, e_2 . Thus, its observation points to the need for a multiband (three or more) model in order to obtain a correct assignment of the bands and their respective couplings.

The total change in the electronic specific heat is compared to the experimentally determined data (open circles) in Fig. 5(c). The agreement between the Eliashberg model and the data is good given the simplicity of the model. However, we obtain a total electron-boson coupling in the intermediate regime. The fitted values of the partial DOS for each band are (in eV^{-1}) $N_1(0) = 0.71, N_2(0) = 3.80,$ and $N_3(0) = 0.59$. The dimensionless coupling constants are $\lambda_{ph} = \lambda_{11} = \lambda_{22} = \lambda_{33} = 0.45, \lambda_{23} = -0.1, \lambda_{13} = -1.0, \lambda_{12} = 0,$ and the interband balance relation $\lambda_{ji}N_j(0) = \lambda_{ij}N_i(0)$ was imposed. These values result in a total average coupling $\lambda_{av} = \sum_{ij}(N_i(0)/N_{\text{tot}})|\lambda_{ij}| = \lambda_{ph} + 2(|\nu_1\lambda_{13} + \nu_2\lambda_{23}|) = 0.88$, where the phenomenological normalized partial DOS $\nu_{\alpha} = N_{\alpha}(0)/N_{\text{tot}}(0)$ have been introduced. This value is significantly smaller than the average coupling constant $\lambda_{av} \approx 2$ obtained for $\text{Ba}_{0.68}\text{K}_{0.32}\text{Fe}_2\text{As}_2$ and other pnictides [1]. Finally, if we neglect the e-ph interaction, we obtain $T_c = 21.7$ K. Similarly, if we neglect the spin fluctuations, we obtain a $T_c = 5.4$ K. This indicates that the phonons produce a nonlinear enhancement of T_c when operating in conjunction with a dominant spin fluctuation mechanism, similar to that proposed for the cuprates [40].

As mentioned previously, multiple scenarios can be considered when making assignments between our effective three-band model and the five bands crossing the Fermi level in the real material. In the following section, we will discuss these scenarios in the context of our our DFT calculations.

Scenario I. One naively takes the $i = 1$ band to represent a combined contribution from the inner two hole bands (denoted h_1 and h_2), while the $i = 2$ band represents the third hole band h_3 and $i = 3$ represents the combined electron pockets $e_{1,2}$.

Scenario II. The second hole band h_2 and the outer electron band e_1 form the strongly coupled bands 1 and 3 that are responsible for the s_{\pm} symmetry, while the remaining two hole bands h_1 and h_3 , together with the second electron band e_2 , form the effective weakly coupled band 2.

Scenario III. The two electron bands e_1 and e_2 would belong to different symmetries or their gap structure is highly anisotropic with a large value on the outer part e_1 and a small value on e_2 . Then the electron band with the small gap, together with the hole bands h_1 and h_3 , would be lumped in that effective weakly coupled band 2. Alternatively, the large PDOS of band 2 should be ascribed to a specific high-energy renormalization acting on the orbitals contributing essentially to the largest hole band h_3 .

Recent ARPES measurements [41] have observed an additional hole-type FSS near the X point sometimes denoted as the propeller blade or ε -FSS. We would like to suggest that this Fermi surface may be affected by surface effects. Such a point of view is supported by a significant difference in

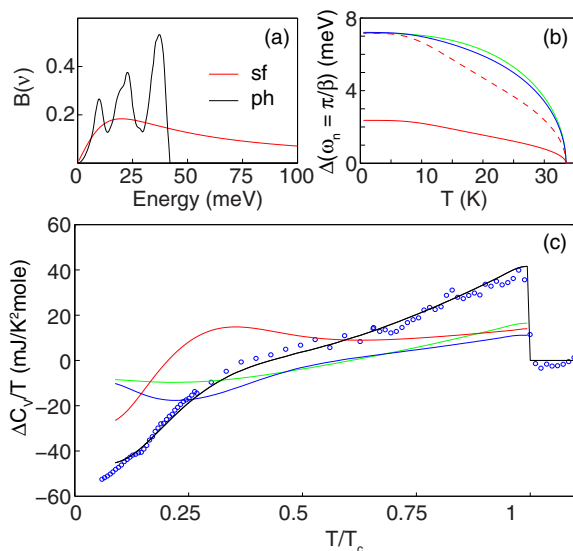


FIG. 5. (Color online) (a) The assumed spectrum of phonons (black/dark) and spin fluctuations (red/light). (b) The temperature dependence of the gap functions $\Delta_i(\omega_n = \pi/\beta)$. The dashed red line in (b) is a rescaled version of the solid red line, to show the non-BCS-like temperature dependence of the superconducting gap for this band (see main text). (c) A comparison between the calculated (thick black line) and measured (open \circ) change in electronic specific heat $\Delta C_{el}(T)$ as a function of the reduced temperature T/T_c . The individual band contributions are also shown for $T < T_c$, following the color scheme of (b).

the cross sections reported for an analogous propeller FSS in KFe_2As_2 , as observed by ARPES [44] and dHvA [42] measurements where a ratio ~ 2 (i.e., from 1.91 to 2.44) has been reported. Since the dHvA data are expected to measure bulk properties, one might conclude that the ARPES data exhibit a larger propeller cross section due to a relaxed lattice structure near the surface. Within LDA the propeller Fermi surface occurs in the very vicinity of stoichiometry KFe_2As_2 , and the corresponding Lifshitz transition for the ε -FSS might take place at higher doping ratios beyond the optimal doping between $x = 0.7$ and 0.9 [43]. Therefore another possible reason of the observed additional FSS observed in an ARPES study is that the doping level of the sample in Ref. [41] is actually higher than in our study. In this context, the lower T_c of about 31 K for the sample investigated in Ref. [41] might be relevant. Further theoretical and experimental studies are necessary to settle this issue, which is of interest for all hole doped 122 systems.

D. Theoretical aspects of normal state properties

We now consider the intermediate coupling strength inferred from our Eliashberg analysis in the context of the total mass enhancement for the Ca-122 system. For this purpose, the DOS $N(\omega)$ and the Fermi surface (FS) topology are required. We will adopt the electronic structure calculated within density functional theory and the local density approximation (LDA) as close to a bare electronic structure without important many-body corrections (see Fig. 6). Our aim is to compare the empirically determined Sommerfeld constant γ_{el} in the electronic specific heat to the value bare value γ_b determined from the bare reference DOS at the Fermi level $N(\omega = 0)$,

$$\gamma_b = \frac{\pi^2 k_B^2}{3} N(0) = 2.5352 N(0), \quad (5)$$

where γ_b is measured in units of mJ mol K^2 (f.u.) and $N(0)$ is measured in states/eV mol . In this way, we can estimate the total mass enhancement due to high-energy correlations and electron-boson coupling.

Using the structural data for $\text{Ca}_{0.34}\text{Na}_{0.66}\text{Fe}_2\text{As}_2$ [45], being very close to the composition of our single crystal, we arrive at $N(0) = 4.69$ states/eV/f.u. or $\gamma_b = 10.96$ mJ/K^2 . Here, the Na doping has been treated within the standard virtual crystal approximation. From our calculated plasma frequencies of 3.15 eV (in-plane) and 1.94 eV (out-of-plane), a relatively small mass anisotropy of 2.64 is found. From this, we estimate an anisotropy for the upper critical fields of 1.63 (in a single-band approximation), which compares reasonably well with available experimental values of 1.85 ± 0.05 for $x = 0.75$ and 1.82 for $x = 0.5$, respectively [3]. The total mass enhancement factor can be estimated from the specific heat data reported here as $\gamma_{el}/\gamma_b \approx 4.95$. This value compares very well with that obtained from the experimental (significantly renormalized) Fermi velocities of 5.06×10^6 cm/s for both $x = 0.5$ and 0.75 [3,46] when compared to the averaged bare Fermi velocity of 2.44×10^7 cm/s obtained from our LDA calculations.

The mass enhancement can also be estimated from the slope of the upper critical field. From our data we find $-dH_{c2}^{(c)}/dT = 5.5$ T/K, which exceeds the reported values of 4 T/K [3] and 4.5 T/K [45] for $x = 0.75$ and 0.66, respectively (obtained

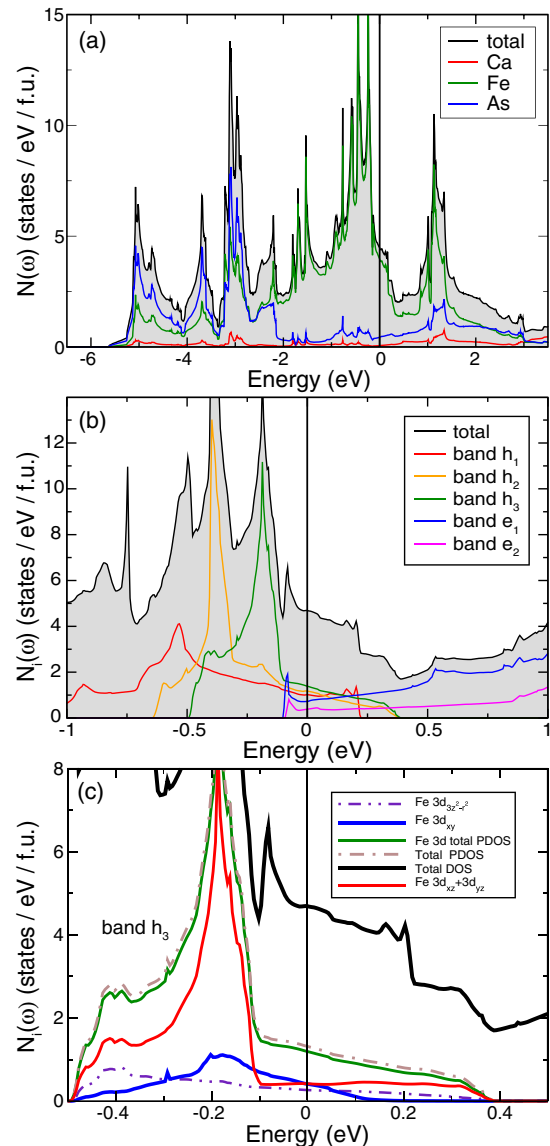


FIG. 6. (Color online) (a) The electronic density of state (DOS) from LDA-FPLO calculation for $\text{Ca}_{0.32}\text{Na}_{0.68}\text{Fe}_2\text{As}_2$ with the various elemental contributions from Fe $3d$, As $4p$, and Ca $4s$ states. (b) The Fermi surface sheets (FSSs) band-resolved contributions. Bands $h_{1,3}$ include the three hole-type FSSs centered around the Γ point (see Fig. 7) and $e_{1,2}$ are the two electron-type FSSs (see Fig. 8), respectively. (c) Orbital resolved partial DOS for the outer hole FSSs h_3 (see Fig. 7), lower panel). The $3d_{xz}$ and $3d_{yz}$ are degenerate in the present tetragonal symmetry and have the same weight. The notation of orbitals is the same as that used in the ARPES and dHvA literature for Fe pnictides, i.e., there is a 45° rotation of the x and y axes with respect of the original tetragonal axis of the the Bravais cell.

from resistivity measurements). For our value of -5.5 T/K for $H_{c2}^{(c)}$, a renormalization factor of 5.56 for $x = 0.68$ is obtained, which is comparable to the values 4.83 derived from the data of Ref. [3] and 5.02 derived from Ref. [45]. Thus we estimate the total mass renormalization for Na-doped Ca-122 to be of order five.

The total mass renormalization is the product of both the low-energy electron-boson (e-b) and high-energy

electron-electron (e-e) interactions. In order to isolate approximately the contributions from the two, we employ a simple factorization ansatz [47]:

$$\gamma_{\text{el}} = \gamma_b(1 + \lambda_{b,\text{tot}})\eta, \quad (6)$$

where $\eta = 1 + \lambda_{e-e}$ describes the effective high-energy renormalization from Coulomb and Hund's interactions that are responsible for the well-known band narrowing observed in photoemission spectroscopies. The low-energy effects from the interaction of conduction electrons with bosonic excitations, such as low-energy spin-fluctuations or phonons, contribute to $\lambda_{b,\text{tot}}$. If we adopt a usual high-energy renormalization for 3d-transition metal compounds $\eta \approx 2.5-3$ [48,49], say 2.6–2.7 [50], then we are left with a constraint for the total bosonic energy renormalization ranging from 1.738 to 1.902, i.e.,

$$\lambda_{b,\text{tot}} \approx 0.82 \pm 0.15, \quad (7)$$

for the total electron-boson coupling constant averaged over all Fermi surface sheets (FSS). Such a value of $\lambda_{b,\text{tot}}$ is in the intermediate coupling regime and agrees well with the value obtained in our multiband Eliashberg analysis. The high-energy renormalization η , which stems from the sizeable Coulomb interaction and/or the Hund's rule coupling (see, e.g., Ref. [49]), is outside the energy region treated in the standard Migdal-Eliashberg theory.

We note that since the title compound is considered within a multiband approach, adopting a single parameter for the description of the high-energy renormalization means that all bands are considered to be renormalized uniformly in the same way. However, in case of correlated multiorbital systems like the A-122 systems this can be violated. For example, bands with a significant contributions from the $3d_{xy}$ orbitals can show a much stronger renormalization close to a Mott transition (orbital selective Mottness) [51].

IV. DISCUSSION

A number of additional comments regarding our Eliashberg result are in order. First, the partial DOS for the second hole pocket, which we associate with band h_3 in scenario I is rather large: it is twice as large as the relative weight from our LDA results (see Figs. 7 and 8). The discrepancy can be considerably reduced if the h_3 band would be upshifted by ≈ 100 meV. Since the h_3 band is dominated by $3d_{xy}$ states, it is most sensitive to many-body effects beyond the LDA. If one assumes a twice as large partial DOS for the h_3 band, the total bare DOS would increase too, reducing our estimate for the total mass renormalization to 3.71 [see Eq. (2)]. Then, adopting a slightly smaller high-energy renormalization $\eta = 2$, we again arrive at a bosonic factor of 1.85, i.e., a total coupling constant $\lambda_{\text{tot}} = 0.85$ in accord with our Eliashberg-theory result of 0.88. Optical measurements yielding the renormalized plasma frequency would be helpful to support such a scenario. Comparing the empirically obtained partial DOS obtained from our model to those obtained in our LDA calculations we again estimate the high-energy $\lambda_{e-e} \approx 1.2$, i.e., somewhat smaller than 1.6 suggested from the adopted values for the plasma frequency. From the other side, a ‘‘corrected’’ band structure, with slightly shifted bands introduced to reproduce

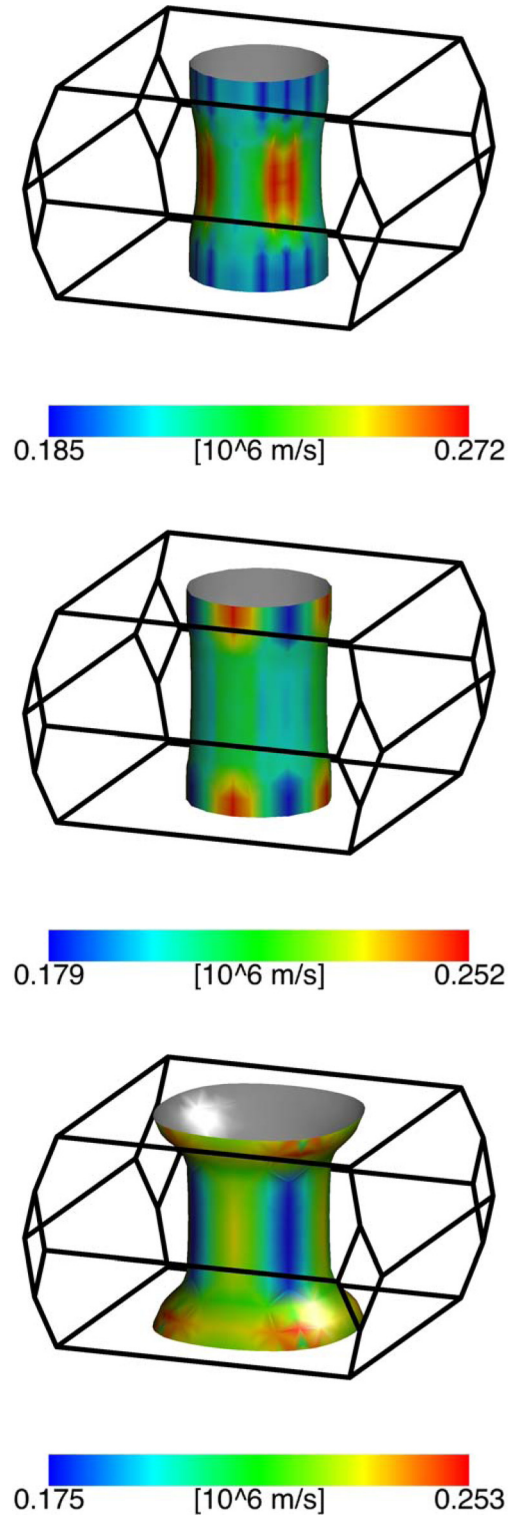


FIG. 7. (Color online) The three hole Fermi surface sheets (FSSs) around the Γ point formed by the bands h_1 (upper), h_2 (middle), and h_3 (bottom) according to our LDA calculation. The color denotes the magnitude of the Fermi velocities. Within scenario I, we tentatively assign the upper (h_1) and the middle (h_2) FSSs to band 1 in our three-band Eliashberg analysis (see subsection D) and the lower FSS (h_3) to band 2. Within scenario II, the band h_2 , only, forms band 1, whereas the two remaining hole bands h_1 and h_3 form the effective band 2. The color scale denotes the magnitude of the calculated Fermi velocities.

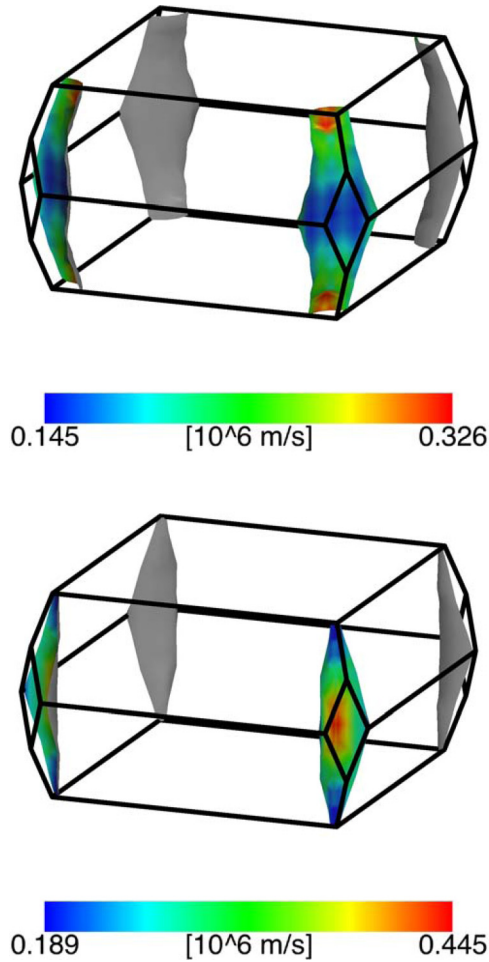


FIG. 8. (Color online) The two electron FSSs resulting from bands e_1 and e_2 according to both scenarios I and II are tentatively assigned to the effective band 3 in our Eliashberg analysis of the specific heat (see Sec. III D).

the FSS cross sections, might result in somewhat different numbers. Adopting now a possibly more realistic “average” value of $\lambda_{e-e} \approx 1.4$, one would arrive at $\lambda_{e-b} \approx 1.06$, which is of the same order as the value obtained above and still well within the intermediate coupling regime.

Second, the relatively weak coupling between the second effective hole pocket and the electron bands, as well as the relatively large contribution from the intraband coupling, implies that the weakly coupled band becomes superconducting at $T = T_c$ via a proximity effect. In the absence of interband coupling, this band would have a much lower T_c . This situation was required in order to reproduce the pronounced knee in ΔC_{el} near $T/T_c \approx 0.3$. If a strong interband coupling is assumed between these bands, or if the intraband coupling is reduced, this knee is significantly muted [1, 13].

Third, the averaged intraband coupling constant of $\lambda_{ph} = 0.45$ is comparable to the repulsive interband counter part of $\lambda_{sf} = 0.446$. The former exceeds the estimates of $\lambda_{ph} \approx 0.2$ based on standard LDA-based calculations for the La-1111 system [52] by slightly more than a factor of two. At the moment it is unclear to what extent this is a specific property of the Ca-122 compounds or a more general many-body driven

enhancement e.g. vertex corrections for the e-ph interaction due to orbital fluctuations [53] or residual correlation effects beyond the LDA, as suggested for the high- T_c cuprates [40, 54–56]. In the context of the Ca-122 derived systems it is also noteworthy that a somewhat enlarged electron-phonon coupling constant $\lambda_{ph} \approx 0.37$ – 0.38 has been reported for Co-doped Ca-122 from first-principles calculations [10]. Finally, a different symmetry of the order parameter (beyond the scope of the present paper) such as $s_{\pm} + id$, nodal d -wave, or s_{\pm} symmetry with accidental nodes are expected at least for the vicinity to the overdoped case near $x = 1$, where all electron Fermi surfaces might disappear. Such a case probably requires a somewhat larger λ_{av} to reproduce the same experimental T_c .

In the context of a non-negligible intraband electron-phonon interaction, the recent four-band analysis of LiFeAs by Ummarino *et al.* [15] is very interesting. These authors calculated first the phonon part of the Eliashberg function and treated the e-ph coupling strength as a fitting parameter, similar to our approach. But the resulting significant intraband interaction was assigned to a single band, only, in contradiction with recent ARPES data [57, 58], which points to phonon features on all four FSSs. Furthermore, the partial DOS $\nu_i = N_i(0)/N(0)$ were adopted from the LDA calculations, at variance with our approach treating them as adjustable parameters. In order to reproduce the observed largest gap of 5 meV on the inner hole-pocket’s FSS, a relatively large intraband coupling constant $\lambda_{11} \approx 0.9$ was required. The authors interpreted their results as a fictitious effect due to the violation of Migdal’s theorem in narrow bands with small Fermi energies. Here, recent NMR measurements in the oxygen free Co-doped Ca-1111 systems are of interest, since the presence of both spin and orbital fluctuations has been claimed in the interpretation of the data [59]. The relevance of a sizable intraband interaction has been stressed in Ref. [60]. Finally, the recently discussed nonmagnetic impurity driven $s_{\pm} \rightarrow s_{++}$ transition at a still sizable T_c [61] makes sense for a considerable intraband coupling.

V. SUMMARY AND CONCLUSIONS

We have examined the electronic specific heat data of good-quality single crystals of $\text{Ca}_{0.32}\text{Na}_{0.68}\text{Fe}_2\text{As}_2$ ($T_c = 34$ K). The low-temperature data in the superconducting state are well described by an effective three-band model with an s_{\pm} symmetry for the superconducting order parameter and comparable Fermi surface averaged intra- and interband coupling strengths. From our model we obtain gap values of $|\Delta| \approx 2.35, 7.48,$ and 7.5 meV. This is in close agreement with recent ARPES measurements [41] where 2.3 and 7.8 meV were reported for the outer and the inner FSSs, respectively. However, the same large gap has been observed in ARPES measurements for an additional holelike FSS. To understand this discrepancy, further theoretical and experimental studies are necessary, which is of interest for all hole doped 122 systems. It should be noted that the magnitude of the gaps on the inner hole and inner electron FSSs are difficult to resolve experimentally within ARPES. Within the different scenarios for the band assignments considered here, different interpretations are possible. In scenario I, large gaps would be present on the inner hole FSSs h_1 and h_2 and on the

TABLE I. Empirical and LDA partial density of states $\nu_i(0) = N_i(0)/N(0)$ $i = 1, 2, 3$ at the Fermi level (PDOS) for scenarios I, II, and III discussed in the text.

PDOS	Eliashberg fit	I	II	III
$\nu_1(0)$	0.139	0.467	0.250	0.250
$\nu_2(0)$	0.745	0.296	0.513	0.595
$\nu_3(0)$	0.116	0.237	0.237	0.155
$\nu_1(0)/\nu_3(0)$	1.203	1.974	1.057	1.404

two electron FSSs $e_{1,2}$, while the small gap would appear on the outer hole FSS h_3 . In scenario II, the large gaps would appear on h_2 and e_2 , while the smaller gap appears on the remaining bands. A similar assignment would be made for scenario III. Scenario II provides the best agreement with the LDA-derived ratios for the PDOS (see Table I). However, the presence of a symmetry breaking mechanism making e_1 and e_2 nonequivalent remains unclear at present. Other experimental probes such as optical conductivity might be helpful to resolve this question, along with further theoretical calculations within a four or five-band models.

The remaining small deviations of about 0.3 meV between the two large gap-values reported in Ref. [41] and our predictions might be ascribed to a slight enhancement of the interband coupling at low temperature as expected in a self-consistent T -dependent treatment of the spin fluctuations (i.e., the formation of a resonance mode in the superconducting state) and/or some gap anisotropy. Observations of the latter have been made for the outer hole-type FSS. Both effects are neglected in our current approach. Alternatively, it can be related to a slightly higher doping level of the sample in Ref. [41] compared to one used in our study.

From our fit of the electronic specific heat, we obtained a total electron-boson coupling constant, averaged over all Fermi surface sheets, with $\lambda_{\text{tot}} \approx 0.9$. Furthermore, a sizable amount of the total coupling is provided by intraband e-ph coupling with $\lambda_{\text{ph}} \approx 0.45$. This value is enhanced compared to the value typically obtained by density functional theory calculations. This implies that the value of T_c in the Na-doped Ca-122 systems is enhanced by the attractive intraband coupling. The value of λ_{tot} is in excellent agreement with the value estimated from the renormalized Sommerfeld constant of the electronic specific heat of about 53 mJ/K² mol (f.u.). This points to moderate or weak coupling with $\lambda \approx 0.9$, only, as discussed in section III.C. We stress once more that the high-energy renormalization typical for itinerant 3d metals yields a larger contribution (≈ 2.6) than the total bosonic one ($1 + \lambda_b \approx 1.82 \pm 0.15$, or $\lambda_b < 1$).

Finally, both the specific heat and the upper critical field data provide a significant total mass renormalization of the order of five including both bosonic and high-energy renormalizations. For a full understanding of the gap structure and the nature of superconductivity of the Na-doped Ca-122 system, further studies on materials with different doping levels are required.

Note added in proof. A recent Mössbauer and muon-spin relaxation study by some of the authors and coworkers has obtained gap values in support of the ones obtained here. This study infers values for the penetration depth that exclude

strong coupling to the bosonic spectrum, in support of our conclusions. The reported values of the anisotropic penetration depths also point to an usually small mass anisotropy like that discussed in the main text. More importantly, these authors found coexisting superconductivity and stripe-type antiferromagnetism at the high Na concentration ($x = 0.5$). The highest T_c occurs in the vicinity of the completely suppressed SDW-state, similar to other pnictide families. This observation provides additional support for our adopted dominant spin fluctuation based interband driven pairing mechanism [65].

ACKNOWLEDGMENTS

The authors thank D. Efremov, J. van den Brink, D. V. Evtushinsky, V. B. Zabolotnyy, S. Borisenko, and G. Prando for useful discussions as well as M. Deutschmann, S. Müller-Litvanyi, R. Müller, J. Werner, S. Pichl, K. Leger, and S. Gass for technical support. This work was supported by the DFG through SPP 1458 and Grants No. GR3330/2 and No. BE1749/13. B.B., C.H., and S.W. acknowledge the research training group GRK 1621. B.B. further acknowledges funding provided by the DFG Projects BE1749/13 and NU887/15-1 and S.W. further acknowledges funding provided by the DFG in the project WU 595/3-1. S.J. acknowledges financial support from the Foundation for Fundamental Research on Matter (FOM, The Netherlands). V.G. thanks funding from the EU-Japan Project (No. 283204 SUPERIRON).

APPENDIX

In adopting Eq. (6), the “true” electron-boson interaction is somewhat underestimated as compared with a more natural description [62]

$$\gamma_{\text{el}} = (1 + \lambda_{\text{e-b}} + \lambda_{\text{e-e}}) \gamma_b, \quad (\text{A1})$$

if $\lambda_{\text{e-e}} > 0$. Using the electron-electron (e-e) self-energy $\Sigma_{\text{e-e}}(\omega)$, the true e-e coupling constant is given by

$$\lambda_{\text{e-e}} = - \left. \frac{\partial \text{Re} \Sigma_{\text{e-e}}}{\partial \omega} \right|_{\omega=0}. \quad (\text{A2})$$

The advantage of adopting Eq. (6) is the possibility to use standard Eliashberg theory to extract $\lambda_{\text{b,tot}}^{\text{eff}}$ from the analysis of low-temperature thermodynamical properties such as specific heat, penetration depth, etc. If instead Eq. (A1) is used, phenomenological model assumptions for the corresponding e-e self-energy $\Sigma_{\text{e-e}}$ have to be adopted [62]. Iwasawa *et al.* (Ref. [63]) proposed a simple expression

$$\Sigma_{\text{e-e}}(\omega) = \frac{g\omega}{(\omega^2 + i\gamma^2)^2}, \quad (\text{A3})$$

where $g = 0.5\beta\gamma^2$ with $\gamma \approx U_d$ (the screened on-site Coulomb interaction) and β as an empirical factor. Within this model one obtains from Eq. (A2)

$$\lambda_{\text{e-e}} = 0.5\beta U_d. \quad (\text{A4})$$

From the analysis of ARPES data for the 4d oxide Sr_2RuO_4 , these authors arrived at $\lambda_{\text{e-e}} = 1.6$ to 1.9 adopting $U_d = 1.2$ to 1.5 eV and $\beta \approx 2.53 \text{ eV}^{-1}$ for the latter value. In case of Fe pnictides, a slightly larger on-site Coulomb interaction is expected and we adopt $U_d \approx 2 \text{ eV}$. Then with the same or a

slightly enhanced β value of 3 eV^{-1} one arrives at slightly larger e-e and e-b coupling constants $\lambda_{e-e} = 2.53$ to 3 and $\lambda_{e-b} \approx 1.5$ to 1, respectively, using the empirical total mass

enhancement of the order of five obtained above in qualitative agreement also with the standard Eliashberg theory based analysis given in the main text.

-
- [1] P. Popovich, A. V. Boris, O. V. Dolgov, A. A. Golubov, D. L. Sun, C. T. Lin, R. K. Kremer, and B. Keimer, *Phys. Rev. Lett.* **105**, 027003 (2010).
- [2] S. Aswartham, M. Abdel-Hafez, D. Bombor, M. Kumar, A. U. B. Wolter, C. Hess, D. V. Evtushinsky, V. B. Zabolotnyy, A. A. Kordyuk, T. K. Kim, S. V. Borisenko, G. Behr, B. Büchner, and S. Wurmehl, *Phys. Rev. B* **85**, 224520 (2012).
- [3] N. Haberkorn, B. Maiorov, M. Jaime, I. Usov, M. Miura, G. F. Chen, W. Yu, and L. Civale, *Phys. Rev. B* **84**, 064533 (2011).
- [4] J. Kim, N. Haberkorn, M. J. Graf, I. Usov, F. Ronning, L. Civale, E. Nazaretski, G. F. Chen, W. Yu, J. D. Thompson, and R. Movshovich, *Phys. Rev. B* **86**, 144509 (2012).
- [5] J. K. Dong, L. Ding, H. Wang, X. F. Wang, T. Wu, G. Wu, X. H. Chen, and S. Y. Li, *New J. Phys.* **10**, 123031 (2008).
- [6] L. Harnagea, S. Singh, G. Friemel, N. Leps, D. Bombor, M. Abdel-Hafez, A. U. B. Wolter, C. Hess, R. Klingeler, G. Behr, S. Wurmehl, and B. Büchner, *Phys. Rev. B* **83**, 094523 (2011).
- [7] K. Kudo, K. Iba, M. Takasuga, Y. Kitahama, J. Matsumura, M. Danura, Y. Nogami, and M. Nohara, *Sci. Rep.* **3**, 1478 (2013).
- [8] M. S. Torikachvili, S. L. Bud'ko, N. Ni, and P. C. Canfield, *Phys. Rev. Lett.* **101**, 057006 (2008).
- [9] R. Mittal, S. Rols, M. Zbiri, Y. Su, H. Schober, S. L. Chaplot, M. Johnson, M. Tegel, T. Chatterji, S. Matsuishi, H. Hosono, D. Johrendt, and Th. Brueckel, *Phys. Rev. B* **79**, 144516 (2009).
- [10] R. Miao, Z. Baj, J. Yang, X. Chen, D. Cai, C. Fan, and L. Wang, *Solid State Commun.* **154**, 11 (2013).
- [11] S.-H. Baek, H.-J. Grafe, L. Harnagea, S. Singh, S. Wurmehl, and B. Büchner, *Phys. Rev. B* **84**, 094510 (2011).
- [12] R. S. Gonelli, M. Tortello, D. Daghero, R. K. Kremer, Z. Bukowski, N. D. Zhigadlo, and J. Karpinski, *Supercond. Sci. Technol.* **25**, 065007 (2012).
- [13] L. Benfatto, E. Cappelluti, and C. Castellani, *Phys. Rev. B* **80**, 214522 (2009).
- [14] M. Tortello, D. Daghero, G. A. Ummarino, V. A. Stepanov, J. Jiang, J. D. Weiss, E. E. Hellstrom, and R. S. Gonnelli, *Phys. Rev. Lett.* **105**, 237002 (2010).
- [15] G. A. Ummarino, S. Galasso, and A. Sanna, *J. Phys.: Condens. Matter* **25**, 205701 (2013).
- [16] A. K. Pramanik, M. Abdel-Hafez, S. Aswartham, A. U. B. Wolter, S. Wurmehl, V. Kataev, and B. Büchner, *Phys. Rev. B* **84**, 064525 (2011).
- [17] V. Grinenko, D. V. Efremov, S.-L. Drechsler, S. Aswartham, D. Gruner, M. Roslova, I. Morozov, K. Nenkov, S. Wurmehl, A. U. B. Wolter, B. Holzapfel, and B. Büchner, *Phys. Rev. B* **89**, 060504(R) (2014).
- [18] K. Koepfner and H. Eschrig, *Phys. Rev. B* **59**, 1743 (1999); I. Opahle, K. Koepfner, and H. Eschrig, *ibid.* **60**, 14035 (1999); see also <http://www.fpllo.de>
- [19] J. P. Perdew and Y. Wang, *Phys. Rev. B* **45**, 13244 (1992).
- [20] D. Kasinathan, M. Wagner, K. Koepfner, R. Cardoso-Gil, Y. Grin, and H. Rosner, *Phys. Rev. B* **85**, 035207 (2012).
- [21] A. A. Golubov, J. Kortus, O. V. Dolgov, O. Jepsen, Y. Kong, O. K. Andersen, B. J. Gibson, K. Ahn, and R. K. Kremer, *J. Phys.: Condens. Matter* **14**, 1353 (2002).
- [22] F. Marsiglio, M. Schossmann, and J. P. Carbotte, *Phys. Rev. B* **37**, 4965 (1988).
- [23] R. Klingeler, N. Leps, I. Hellmann, A. Popa, U. Stockert, C. Hess, V. Kataev, H.-J. Grafe, F. Hammerath, G. Lang *et al.*, *Phys. Rev. B* **81**, 024506 (2010).
- [24] Z.-S. Wang, H.-Q. Luo, C. Ren, and H.-H. Wen, *Phys. Rev. B* **78**, 140501 (2008).
- [25] B. Shen, H. Yang, Z.-S. Wang, F. Han, B. Zeng, L. Shan, C. Ren, and H.-H. Wen, *Phys. Rev. B* **84**, 184512 (2011).
- [26] K. Zhao, Q. Q. Liu, X. C. Wang, Z. Deng, Y. X. Lu, J. L. Zhu, F. Y. Li, and C. Q. Jin, *J. Phys.: Condens. Matter* **22**, 222203 (2010).
- [27] N. Ni, S. Nandi, A. Kreyssig, A. I. Goldman, E. D. Mun, S. L. Budko, and P. C. Canfield, *Phys. Rev. B* **78**, 014523 (2008).
- [28] F. Ronning, T. Klimczuk, E. D. Bauer, H. Volz, and J. D. Thompson, *J. Phys.: Condens. Matter* **20**, 322201 (2008).
- [29] R. F. J. E. Gordon, M. L. Tan, and N. Phillips, *Solid State Commun.* **69**, 625 (1989).
- [30] R. J. McQueeney, S. O. Diallo, V. P. Antropov, G. D. Samolyuk, C. Broholm, N. Ni, S. Nandi, M. Yethiraj, J. L. Zarestky, J. J. Pulikkotil, A. Kreyssig, M. D. Lumsden, B. N. Harmon, P. C. Canfield, and A. I. Goldman, *Phys. Rev. Lett.* **101**, 227205 (2008).
- [31] K. Gofryk, A. S. Sefat, E. D. Bauer, M. A. McGuire, B. C. Sales, D. Mandrus, J. D. Thompson, and F. Ronning, *New J. Phys.* **12**, 023006 (2010).
- [32] F. Hardy, P. Burger, T. Wolf, R. A. Fisher, P. Schweiss, P. Adelmann, R. Heid, R. Fromknecht, R. Eder, D. Ernst, H. v. Löhneysen, and C. Meingast, *Europhys. Lett.* **91**, 47008 (2010).
- [33] G. Mu, H. Luo, Z. Wang, L. Shan, C. Ren, and H.-H. Wen, *Phys. Rev. B* **79**, 174501 (2009).
- [34] J. Paglione and R. L. Greene, *Nat. Phys.* **6**, 645 (2010).
- [35] S. L. Bud'ko, N. Ni, and P. C. Canfield, *Phys. Rev. B* **79**, 220516(R) (2009).
- [36] C. P. Poole, Jr., H. A. Farach, R. J. Creswick, and R. Prozorov, *Superconductivity*, 2nd ed. (Academic Press, Amsterdam, 2007).
- [37] H. Fukazawa, Y. Yamada, K. Kondo, T. Saito, Y. Kohori, K. Kuga, Y. Matsumoto, S. Nakatsuji, H. Kito, P. M. Shirage, K. Kihou, N. Takeshita, C.-H. Lee, A. Iyo, and H. Eisaki, *J. Phys. Soc. Jpn.* **78**, 083712 (2009).
- [38] F. Hardy, T. Wolf, R. A. Fisher, R. Eder, P. Schweiss, P. Adelmann, H. v. Löhneysen, and C. Meingast, *Phys. Rev. B* **81**, 060501(R) (2010).
- [39] A. J. Millis, *Phys. Rev. B* **45**, 13047 (1992).
- [40] S. Johnston, F. Vernay, B. Moritz, Z.-X. Shen, N. Nagaosa, J. Zaanen, and T. P. Devereaux, *Phys. Rev. B* **82**, 064513 (2010).
- [41] D. V. Evtushinsky, V. B. Zabolotnyy, L. Harnagea, A. N. Yaresko, S. Thirupathiah, A. A. Kordyuk, J. Maletz,

- S. Aswartham, S. Wurmehl, E. Rienks, R. Follath, B. Büchner, and S. V. Borisenko, *Phys. Rev. B* **87**, 094501 (2013).
- [42] T. Terashima, N. Kurita, M. Kimata, M. Tomita, S. Tsuchiya, M. Imai, A. Sato, K. Kihou, C.-H. Lee, H. Kito, H. Eisaki, A. Iyo, T. Saito, H. Fukazawa, Y. Kohori, H. Harima, and S. Uji, *Phys. Rev. B* **87**, 224512 (2013).
- [43] N. Xu, P. Richard, X. Shi, A. van Roekeghem, T. Qian, E. Razzoli, E. Rienks, G.-F. Chen, E. Ieki, K. Nakayama, T. Sato, T. Takahashi, M. Shi, and H. Ding, *Phys. Rev. B* **88**, 220508(R) (2013).
- [44] T. Yoshida, S. Ideta, I. Nishi, A. Fujimori, M. Yi, R. G. Moore, S. K. Mo, D.-H. Lu, Z.-X. Shen, Z. Hussain, K. Kihou, P. M. Shirage, H. Kito, C. H. Lee, A. Iyo, H. Eisaki, and H. Harima, [arXiv:1205.6911](https://arxiv.org/abs/1205.6911).
- [45] K. Zhao, Q. Q. Liu, X. C. Wang, Z. Deng, Y. X. Lv, J. L. Zhu, F. Y. Li, and C. Q. Jin, *Phys. Rev. B* **84**, 184534 (2011).
- [46] The Fermi velocities in Ref. [3] were estimated from an upper critical field analysis assuming a single-band Ginzburg-Landau and BCS theory.
- [47] Recently, Iwasawa *et al.* (Ref. [63]) have presented a more involved discussion regarding estimating λ_{e-b} in systems with significant correlation effects. Adopting their approach does not change our discussion significantly, as shown in Appendix.
- [48] M. M. Qazilbash, J. J. Hamlin, R. E. Baumbach, L. J. Zhang, D. J. Singh, M. B. Maple, and D. N. Basov, *Nat. Phys.* **5**, 647 (2009).
- [49] Z. P. Yin, K. Haule, and G. Kotliar, *Nat. Mater.* **10**, 932 (2011).
- [50] We have adopted a similar value of η for the related strongly overdoped KFe_2As_2 with a smaller calculated plasma frequency and slightly less screened high-energy interactions (Ref. [64]).
- [51] L. de Medici, G. Giovanetti, and M. Capone, [arXiv:1212.3966v2](https://arxiv.org/abs/1212.3966v2).
- [52] L. Boeri, O. V. Dolgov, and A. A. Golubov, *Phys. Rev. Lett.* **101**, 026403 (2008).
- [53] H. Kontani, T. Saito, and S. Onari, *Phys. Rev. B* **84**, 024528 (2011).
- [54] S. Johnston, I. M. Vishik, W. S. Lee, F. Schmitt, S. Uchida, K. Fujita, S. Ishida, N. Nagaosa, Z.-X. Shen, and T. P. Devereaux, *Phys. Rev. Lett.* **108**, 166404 (2012).
- [55] O. Rösch and O. Gunnarsson, *Phys. Rev. Lett.* **92**, 146403 (2004).
- [56] A. S. Mishchenko and N. Nagaosa, *Phys. Rev. Lett.* **93**, 036402 (2004).
- [57] A. A. Kordyuk, V. B. Zabolotnyy, D. V. Evtushinsky, T. K. Kim, I. V. Morozov, M. L. Kulić, R. Follath, G. Behr, B. Büchner, and S. V. Borisenko, *Phys. Rev. B* **83**, 134513 (2011).
- [58] S. V. Borisenko, V. B. Zabolotnyy, A. A. Kordyuk, D. V. Evtushinsky, T. K. Kim, I. V. Morozov, R. Follath, and B. Büchner, *Symmetry* **4**, 251 (2012).
- [59] S. Tsutsumi, N. Fujiwara, S. Matsuishi, and H. Hosono, *Phys. Rev. B* **86**, 060515(R) (2012).
- [60] M. Kulić, S.-L. Drechsler, and O. V. Dolgov, *Europhys. Lett.* **85**, 47008 (2010).
- [61] D. V. Efremov, M. M. Korshunov, O. V. Dolgov, A. A. Golubov, and P. J. Hirschfeld, *Phys. Rev. B* **84**, 180512(R) (2011).
- [62] H. Iwasawa, Y. Yoshida, I. Hase, K. Shimada, H. Namatame, M. Taniguchi, and Y. Aiura, *Sci. Rep.* **3**, 1930 (2013).
- [63] H. Iwasawa, Y. Yoshida, I. Hase, K. Shimada, H. Namatame, M. Taniguchi, and Y. Aiura, *Phys. Rev. Lett.* **109**, 066404 (2012).
- [64] M. Abdel-Hafiez, S. Aswartham, S. Wurmehl, V. Grinenko, C. Hess, S. L. Drechsler, S. Johnston, A. U. B. Wolter, B. Büchner, H. Rosner, and L. Boeri, *Phys. Rev. B* **85**, 134533 (2012).
- [65] P. Materne *et al.* (private communication).